Spectral processing techniques for efficient monitoring in optical networks

FABIANO LOCATELLI,[1,*] KONSTANTINOS CHRISTODOULOPOULOS,[2] MICHELA SVALUTO MOREOLO,[1] JOSEP M. FÀBREGA,[1] LAIA NADAL,[1] SALVATORE SPADARO[3]

[1]Centre Tecnològic de Telecomunicacions de Catalunya (CTTC/CERCA), Castelldefels (Barcelona), Spain
[2]Nokia Bell Labs, Stuttgart, Germany
[3]Universitat Politècnica de Catalunya, Barcelona, Spain
**Corresponding author: fabiano.locatelli@cttc.es*

Received XX Month XXXX; revised XX Month, XXXX; accepted XX Month XXXX; posted XX Month XXXX (Doc. ID XXXXX); published XX Month XXXX

Having ubiquitous optical monitors in dense wavelength-division multiplexing (DWDM) or flex-grid networks allows the estimation in real time of crucial parameters. Such monitoring would be even more important in disaggregated optical networks, to inspect performance issues related to inter-vendor interoperability. Several important parameters can be retrieved using optical spectrum analyzers (OSAs). However, omnipresent OSAs represents an infeasible solution. Nevertheless, the advent of new, relatively cheap, compact and medium-resolution optical channel monitors (OCMs) enable a more intensive deployment of these devices. In this paper, we identify two main scenarios for the placement of such monitors: at the ingress and at the egress of the optical nodes. In the ingress scenario, we can directly estimate the parameters related to the signals, but not those related to the filters. On the contrary, in the egress scenario, the filter related parameters can be easily detected, but not those related to ASE. Therefore, we present two methods that, leveraging a curve fitting and a machine learning (ML) regression algorithm, allow to detect the missing parameters. We verify the proposed solutions with spectral data acquired in simulation and experimental setups. We obtained good estimation accuracy for both setups and for both studied placement scenarios. Noteworthy, in the experimental assessment of the ingress scenario, we achieved a maximum absolute error (MAE) lower than 1 GHz in filter bandwidth estimation and a MAE lower than 0.5 GHz in filter frequency shift estimation. In addition, by comparing the relative errors of the considered parameters, we identified the ingress scenario as the more beneficial. In particular, we estimated the filter central frequency shift with 84% and the filter 6-dB bandwidth with 75% higher accuracy, with respect to datasheet/reference values. This translates into a total reduction of the estimated signal-to-noise ratio (SNR) penalty, introduced by a single optical filter, of 0.24 dB. © 2020 Optical Society of America

http://dx.doi.org/10.1364/JOCN.99.099999

1. INTRODUCTION

Nowadays, disaggregation is an important trend within optical networks. According to this paradigm, several elements of the network may be provided by different vendors [1]. Therefore, in such situation, advanced vendor-independent monitoring capabilities would be required in order to cope with specification mismatches and performance variations of the disaggregated network elements [2]. More in general, in an optical network, an ideal scenario envisions omnipresent and powerful optical performance monitoring (OPMs), placed before and after every network node. OPMs enable to monitor different parameters across the network [3]. Among them, the most important are the amplified spontaneous emission (ASE) noise, directly related to the optical signal-to-noise ratio (OSNR) and the filter related parameters, such as the filter 3-dB or 6-dB bandwidth and the filters shifts. The OSNR is considered as one of the most important parameters to be monitored, because it is directly correlated to the bit error rate (BER) and it is transparent to the modulation format. Within the different types of OPMs, spectral monitoring is the most interesting option, since it can identify all signal parameters, except for the nonlinear interference related impairments, which are in general extremely hard to monitor [3,4]. Nowadays, cost-effective versions of the classic optical spectrum analyzers (OSAs), also known as optical channel monitors (OCMs), are available on the market [5]. These devices can be considered a cheap solution (often in the order of few hundreds of euros), when compared with the cost of the rest of the network elements in dense wavelength-division multiplexing (DWDM) or flex-grid networks. Despite their low-cost, and except for the frequency drift limitation which affects them in the long term, OCMs show good performance and resolutions (up to sub-GHz order). Therefore, we envision the employment of such monitoring devices, considering their eventual replacement once the frequency drift effects

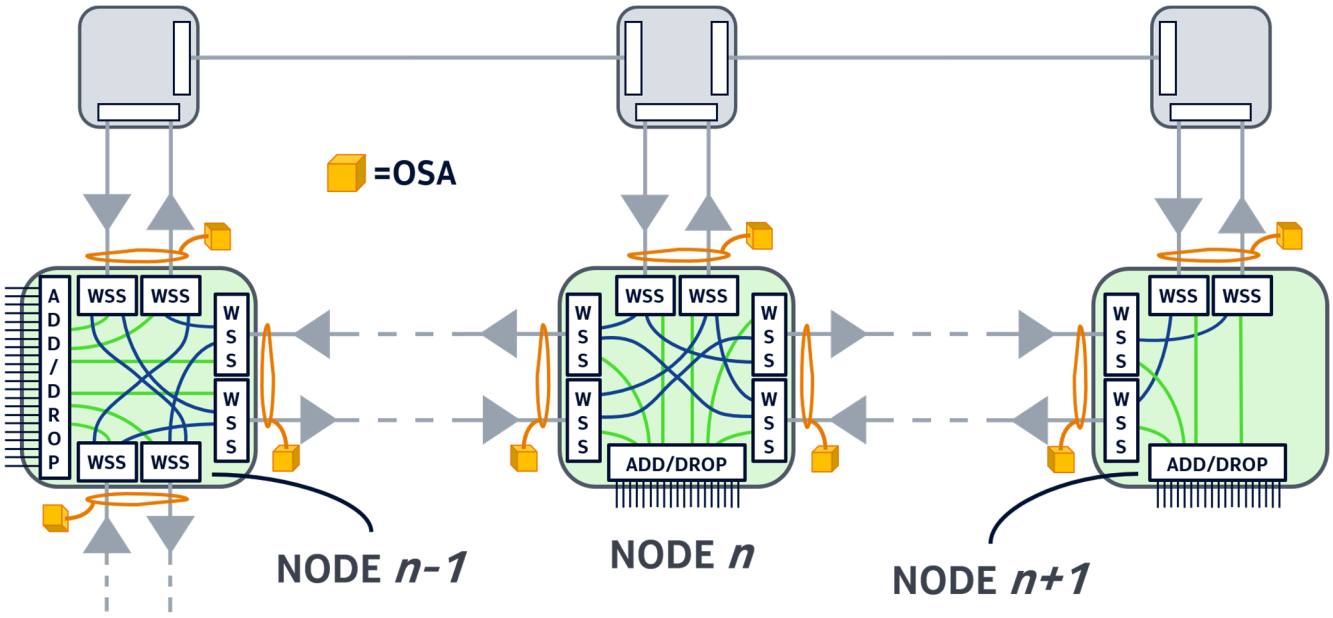

Fig. 1. Ideal scenario where powerful monitors are available at the ingress and egress ports of every node of the network.

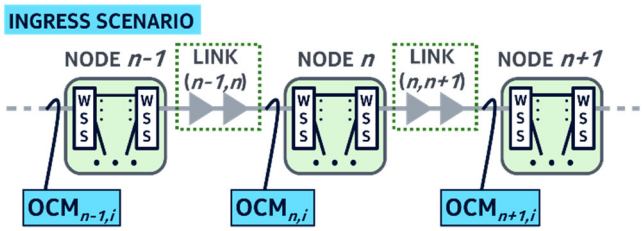

Fig. 2. Ingress scenario. WSS: wavelength selective switch; OCM: optical channel monitor.

make them impractical. All these features could enable a wide use of such monitors throughout the optical network. The most appropriate position to place them is close to the reconfigurable optical add/drop multiplexers (ROADMs), which are key enablers for optical core/metro networks [6].

In deployed wavelength switched optical networks employing DWDM or flexgrid channels, a ROADM allows individual channels (i.e. individual wavelengths) to pass-through the node, or to be added or dropped. So, it allows for the termination and entry of services but also the transparent bypass of the node, avoiding costly optical-electrical-optical conversions [7,8]. In current generation ROADMs, these functions are implemented by means of wavelength selective switches (WSSs). A WSS is an 1x*N* optical device, which allows any entering wavelength on the common input port to be switched to any of the *N* available output ports. The WSS also works in the opposite direction, selecting out of the *N* input ports the channels to be forwarded on the common output port. To do so, the WSSs include optical filters that introduce different filtering penalties on the optical signals [9]. Furthermore, the filters introduce a sharp power drop at the signal sides, which makes the measurement of the ASE noise challenging. In fact, one of the classical ways to measure it are defined as out-of-band methods, since they rely on noise measurements taken outside the signal bandwidth. One example is the interpolation method [10], where the noise levels at the sides of the considered channel spectrum are interpolated to give an estimation of the ASE noise value inside the channel. These kinds of approaches are even more complex to be applied in modern DWDM and flex-grid networks, where the spacing between channels is reduced to the minimum. Indeed, the challenges to face are not only the already mentioned strong filtering, but also the fact that in such networks, each channel exhibits a different noise level, according to the route it has taken. Therefore, new OSNR monitoring techniques which operate in-band, are needed.

In the past few years, ROADM architecture evolved from a "Broadcast and Select" (B&S) approach to a more flexible and better performing paradigm, called "Route and Select" (R&S) [11]. The former employs a broadcasting power splitter and only a single WSS per degree (i.e. per direction) at the egress fiber, yielding reduced filtering penalties at low cost [12]. Contrarily, the R&S approach uses two independent WSSs per degree, both at the ingress and egress fibers and yields better isolation of connections and lower insertion losses. Of course, since R&S has twice the number of WSSs of B&S, it introduces a larger passband narrowing effect and it is a more expensive solution [13].

Several monitoring strategies that use various amount of monitors can be implemented in the network. Of course, the higher the number and the more advanced specifications the deployed monitors have, the more expensive the solution is. In the ideal case, depicted in Fig. 1, powerful spectral monitors are available before, after and inside every node of the network (note that, Fig. 1 does not display the internal monitors). This solution in reality is not feasible because of its cost. Thus, we identified 2 alternative scenarios for the placement of the monitors, limiting/selecting their positioning, in order to reduce the overall cost. The first scenario requires the monitors to be placed before the ingress ports of each ROADM, i.e. before their ingress WSSs, as shown in Fig. 2. In the second scenario the optical monitors are placed after the egress ports of the ROADMs nodes, i.e. after their egress WSSs, as depicted in Fig. 3.

As we previously mentioned, parameters such as the out-of-band OSNR, the total optical power or the wavelength drift can be easily estimated through optical spectrum-based techniques [3]. For example, the already mentioned interpolation method, in which the in-band noise level is estimated interpolating the noise at the two sides of the signal

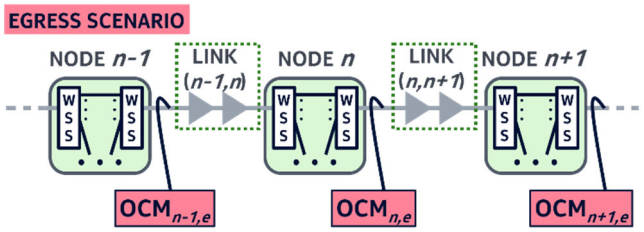

Fig. 3. Egress scenario. WSS: wavelength selective switch; OCM: optical channel monitor.

[10]. Moreover, nowadays, a large amount of advanced analytics/machine learning (ML) methods have emerged, enabling the enhancement of the available spectral data. Thus, from the optical spectrum one can retrieve information not only about the signal itself, but also related to the condition of the network or the elements that compose it, like the optical amplifiers and filters. In [14], for example, the authors proposed three ML-based methods to detect and identify the filter related soft failures, such as filter shift/laser drift and filter tightening. These proposed approaches, rely on a series of frequency-power pairs, retrieved directly from the optical spectra captured with OSAs placed at the egress port of every node of the network. On the other hand, in [15], an alternative solution to OSAs for filter impairments monitoring was presented. There, the authors proposed a center of mass-based approach employed inside the coherent receiver, which essentially operated as an OSA monitor at the end of the connection. Another solution based on monitoring information of existing connections, to estimate filtering uncertainties and therefore improve the quality of transmission (QoT) estimation of future connections, was proposed in [16]. In that paper, the authors, leveraging a ML regression model and processing spectral data acquired with monitors such as OCMs, were able to show, in simulations, an 80% reduction of the margin for a new connection. In [17], optical spectral data analysis was applied to filterless optical networks. The authors, proposed a method to monitor the power fluctuations and laser drifts of the transponders, exploiting optical spectra collected by a single OCM per filterless segment. In [18], the authors compared the performance of 4 different ML algorithms, in particular, support vector machine (SVM), artificial neural network (ANN), k-nearest neighbors (KNN) and decision tree, for estimating parameters, such as central wavelength, OSNR and signal bandwidth, by processing the spectral data. However, in [18], wide optical spectra were considered, which are not available in deployed filtered networks, where only in-band optical spectra can be retrieved from the monitors (i.e. inside the channel created by the filters). Finally, optical spectra processing has also been employed for network security purposes, as in [19], where the authors implemented a ML-based approach able to detect unauthorized signals in the network.

Selecting one of the placement strategies outlined above results in different monitored parameters and in the lack of some others. In the ingress scenario, we can directly estimate the parameters related to the signal such as the ASE noise, but not those related to the filter. On the contrary, in the egress scenario, the filter related parameters can be easily detected, but those related to the ASE noise cannot. To cope with the missing information, we propose to enhance the collected spectra with adequate data analytics and ML methods. Throughout this paper, when we mention the spectral monitored data, we refer to the monitored power spectral density (PSD); we will use these two terms interchangeably.

In our previous works, we proposed a ML-based solution for in-band OSNR monitoring [20,21] in the egress scenario, therefore exploiting optical spectra captured at the node's output. We verified the validity of the proposed solution through simulated and experimental setups. In particular, in [20], we compared the performance of two ML algorithms, SVM and Gaussian process regression (GPR) using optical spectra collected at two different resolutions: at very-high resolution, namely 12.5 MHz, and at a medium resolution, namely 1.25 GHz. We observed good estimation accuracy, while no substantial improvements emerged using the very-high resolution spectra. In addition, in [21], we further verified the approach presented in [20], implementing a new experimental setup, which considered strong filtering conditions and achieved good estimation accuracy. In [22], we focused on the ingress scenario. There, we proposed a method to retrieve the transfer function (TF) of a bandpass optical filter, e.g. of a WSS, exploiting the optical spectra captured at the node's input port. Obtaining the filter TF, allowed us to understand the quality of the filter itself. As for the previous works, we verified the proposed solution with spectral data sets collected through both simulation and experimental setups.

In this paper, we compare the two identified placement scenarios and the related parameters estimation methods. To do so, we provide a thorough overview of the proposed monitoring scenarios. We present in detail the identified data analytics and ML approaches for processing the available spectra and we improve them with respect to our previous works. We also assess them in unified simulation and experimental setups. Finally, after comparing them, we provide guidelines for the preferred one in terms of estimation accuracy improvements and signal-to-noise (SNR) penalty reduction.

The rest of this paper is structured as follows. In Section 2, we present a detailed overview of the two main identified placement scenarios and the developed corresponding processing methods. We then present in Section 3 the implemented simulation setup along with the results. In Section 4, we describe the experimental setup and the related results. In Section 5, we compare the results obtained within the different placement scenarios and we provide some guidelines on their employment. Finally, in Section 6, we summarize the achieved results and conclude the paper.

2. OPTICAL SPECTRAL MONITORS PLACEMENT SCENARIOS AND SPECTRAL PROCESSING METHODS

We focus our attention on the two most important categories of parameters that can be monitored through OPMs, especially in disaggregated optical network scenarios: signal-related and filter-related parameters. The first group includes the signal central frequency, the signal 3/6-dB bandwidth and the ASE noise added to the signal (therefore, its OSNR). The second group is composed of the filter central frequency and the filter 3/6-dB bandwidth. We propose to retrieve such information through spectral monitoring, employing medium-accuracy OCMs. In both the scenarios identified in Fig. 2 and Fig. 3, we were able to neglect the effects of the portion of the network preceding the considered OCM. To do this, after identifying the channel which we are interested in, we would collect the related spectra from the OCM placed at the WSS traversed by that channel. In particular, if we define with OCM_{n+1} the monitor located at the point n+1 of the network, we divided, in the linear domain, the OCM_{n+1} captured PSDs by those captured with OCM_n. This operation allows us to focus only on what happens between the monitor located in position n and the monitor located in the considered position n+1, without any knowledge and any effect of what comes before position n. Performing such divisions along the path of an optical connection (lightpath), enables us to see the effect of each link/node on that path, nullifying those of the previous network elements along that same lightpath. Assuming that no frequency drift affects the employed OCMs, the only requirement for such operation is the collection of both spectra (from OCM_{n+1} and OCM_n) at a single point, which would typically be the central controller. In addition, again assuming no frequency error on the OCM, variations of the spectra resolutions can be easily accounted with some simple processing, e.g.

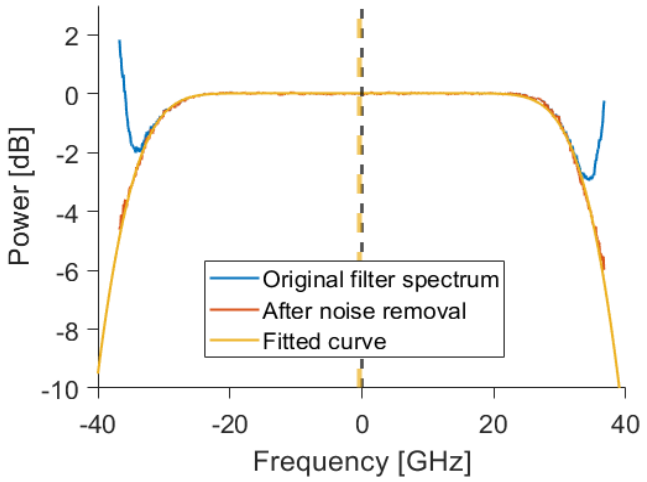

Fig. 4. Example of an experimentally obtained filter TF spectrum before (blue) and after (orange) the noise removal process. The solid yellow plot is the fitted curve, while the dotted yellow line represents the identified central frequency of the fitted curve, which is shifted with respect to the original center (dotted black line).

upsampling the lowest resolution. Moreover, we are constraining the frequency range related to the channel of interest, relying on the spectral grid defined by the ITU-T standards [23]. It is worth noting that in this paper we focus on the extraction of the per link/node parameters of a single connection. Correlating information among connections that cross the same link/node, can improve further the understanding of the link/node features. This would require a further processing/analysis of the outputs of our proposed solution at some centralized point (e.g. the software-defined networking (SDN) controller). Such processing methods are outside the scope of this paper, therefore the reader is referred to [24,25], for various solutions at that processing level. In addition, in this paper we focused our investigation on different transmission aspects, without considering the consequences of the nonlinear interference (NLI) caused by the Kerr effect. In fact, all the spectra we collected and processed for this work referred to a single channel configuration. However, for almost all the investigated cases we will present in the next sections, we considered strong filtering scenarios, thus neglecting the effects of the linear crosstalk coming from any eventual adjacent channels, on the optical spectra. Moreover, since self and cross-channel NLIs only have a minor impact on the spectra, we claim our solutions to be unaffected by such effects.

The two main OCM monitors placement scenarios that we identified, along with the two solutions we propose for retrieving the related missing parameters, are discussed in details in the next subsections.

A. Ingress Monitoring Scenario

In the ingress monitoring scenario, depicted in Fig. 2, the OCMs are placed before the ingress WSS of each ROADM nodes of the network. This translates into a relative ease in retrieving information about the signals entering the node, since they are monitored before they are filtered by the WSSs of the node itself. Therefore, parameters such as the signal central frequency, the signal 3/6-dB bandwidth and the OSNR, can be measured directly or through (mild) processing of the optical spectra collected by the OCMs. On the contrary, the optical spectra collected through such configuration will not give any direct information about the filters, thus some advanced processing is required. In the ideal scenario of Fig. 1 (OCMs everywhere), we would simply divide in the linear domain the PSD captured at the egress port of the node to the one captured at its ingress. As discussed in Section I, depending on the considered ROADM architecture, the number of WSSs contained in a ROADM node, can vary between one (B&S) and two (R&S) per degree. We treat both ROADM architecture the same: if the node contains two filters, we model an equivalent filter for the specific ingress-egress direction. So, by doing the above division, we would obtain the TF of the single filter (B&S) or the equivalent of both filters (R&S) involved in the specific ingress-egress direction. However, since the monitoring placement scenario we are now considering does not have optical monitors at the egress ports, we have to find another way to obtain the egress related PSD. To cope with this lack, we replace the PSD monitored at the egress port, with the one monitored at the ingress of the following node. Referring to Fig. 2, and following the approach proposed in [22], we divide, in the linear domain, the optical spectra captured with $OCM_{n+1,i}$ by the one captured with $OCM_{n,i}$, where n represents a generic node of the optical network, $n+1$ the node following n in the direction of our interest, and $OCM_{n,i}$ and $OCM_{n+1,i}$, represent the OCMs at the ingress port of node n and node $n+1$, respectively. Of course, the result of this division represents not only the filter TF of node n, but also the noise accumulated over the link connecting the two nodes, referred to as link $(n,n+1)$ in Fig. 2. As discussed above, this operation removes the effects accumulated by the connection over its path before reaching the monitor of node n. So we can only focus on the last part, the filter of node n and the link $(n,n+1)$. It is worth noting that when two or more frequency adjacent channels come from the same link and continue at the same link, they can also share the same filter and thus the internal filter edge(s) would not show up in the TF. For such channels our method will not work. On the contrary, when two adjacent channels come from different input ports, or go towards different output ports (including drop ports), the filter edges are visible, and the solution we proposed can be employed.

To identify the noiseless TF of the filter, we can estimate the ASE noise through the $OCM_{n+1,i}$ captured spectrum and remove it, in the linear domain, from the PSD obtained with the aforementioned division. Due to filtering and/or the response of the OCM, measuring the noise at the sides of the spectra might not be very easy. Thus, enhancing what we proposed in [22], we implemented a process that works on the monitored spectra and identifies the noise contribution. The function searches over a set of noise values. They can come from the monitored spectra or from the basic link/span knowledge with the addition of an accuracy correction factor. Then, the function selects the noise amount that resulted in the best (lowest) fitting error. In a sense, it relies on how good the shape of the reference filter matches the shape of the real one. In fact, removing a lower or higher amount of noise would return a wrong filter shape, yielding to a worse match with respect to the case where a correct noise amount is subtracted. The assumption behind the ASE estimation is that the filter at node n suppresses the noise introduced by the amplifiers/links cascade up to that point and therefore, the noise at the sides of the $OCM_{n+1,i}$ collected spectra is mainly due to the link $(n,n+1)$ contribution. This noise identification process allowed us to better estimate the ASE noise, with respect to what we reported in [22]. An example of a TF obtained through the noise removal, starting from experimentally collected spectra, is shown in Fig. 4. Observing the filter TF obtained through the above steps, we see that we are still not able to measure its 6-dB bandwidth, due to the fact that its two sides do not reach deep values. This happens in most cases that we observed with simulation and experimental spectral data and occurs because at the spectra edges we are processing the noise instead of the signal contained in the channel.

To overcome this obstacle, we propose to reconstruct the full TF, by fitting the obtained portion of spectrum with a function that corresponds to the 'ideal' shape of the filter. Typically, optical filters are

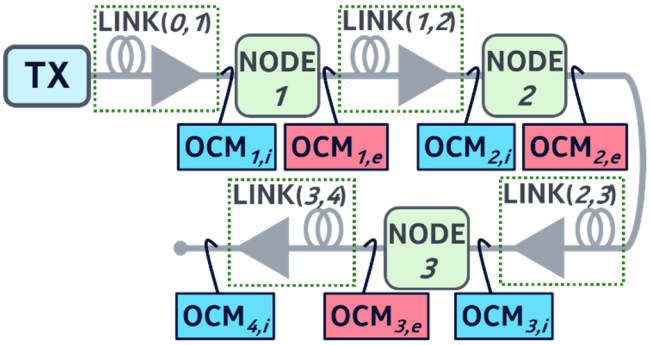

Fig. 5. Scheme of the implemented VPIphotonics simulation setup. TX: transmitter; OCM: optical channel monitor.

considered to have a high-order Gaussian shape. In [26], the authors, leveraging the error function $\mathrm{erf}(x)$, proposed a model for the characterization of the optical field spectrum $S(f)$ of a bandpass filter created by a WSS. The function modeling an ideal filter, which is symmetric and centered at 0 frequency, is the following:

$$S(f) = \frac{1}{2}\alpha\sqrt{2\pi}\left[erf\left(\frac{\beta/2-f}{\sqrt{2}\alpha}\right) - erf\left(\frac{-\beta/2-f}{\sqrt{2}\alpha}\right)\right] \quad (1)$$

where α is the parameter related to steepness of the filter edges (i.e. the filter order), β is the 6-dB bandwidth of the filter and f represents the frequency.

Due to misalignment of filter to the signal (transmitter laser and/or filter shifts) and to power leveling issues, the portions of filter TFs that we want to fit are often not centered. Therefore, to consider the two eventual shifts in the directions of x and y-axis, we extended the Eq. 1 based model with two new parameters: δ and γ, respectively. The equation representing the new model is the following:

$$S(f) = \frac{1}{2}\alpha\sqrt{2\pi}\left[erf\left(\frac{\beta/2-f-\delta}{\sqrt{2}\alpha}\right) - erf\left(\frac{-\beta/2-f-\delta}{\sqrt{2}\alpha}\right)\right] + \gamma \quad (2)$$

where δ represents the shift of the filter central frequency and γ is a normalization factor for the y-axis shifts. By tuning the parameters α, β, γ and δ, we can now fit the obtained portions of filters TFs spectra with the logarithmic squared version of Eq. 2. The range in which the parameters are tuned, can be narrowed down based on the filter specifications. This allows a better fitting and therefore a better estimation of the filter related features. In fact, once the fitting process is over, the values assumed by the parameters β and δ represent the estimated filter 6-dB bandwidth and the estimated filter central frequency shift, respectively. We focused our analysis on the two filter parameters that we considered as the most representative, but essentially we estimate the full shape of the filter TF, thus making any other parameter of interest retrievable. Note that the above model can be also extended to capture filter shape asymmetries, which were not heavily present in our simulated and experimental data. So, we do not report the evaluation of such effects here.

B. Egress Monitoring Scenario

In the egress monitoring scenario, the monitors are placed exclusively after the egress WSS of each optical node of the network, as shown in Fig. 3. From the optical spectra collected with such configuration, we can easily retrieve information regarding the optical filters of the node, but not about the signals entering the node. Filter related parameters can be retrieved because the filter directly affects the signal traversing the node. In fact, by dividing (in the linear domain) the PSD captured with $\mathrm{OCM}_{n+1,e}$ by the one captured with $\mathrm{OCM}_{n,e}$, we obtain the contributions of link (*n,n+1*) and of the filters of node *n+1*. This operation removes the effects of the cascade up to the location of $\mathrm{OCM}_{n,e}$, leaving the filter TF clearly visible, while hiding the signal related parameters, such as the ASE noise. Once the TF is identified, the filter related parameters can be retrieved applying a fitting approach similar to the one proposed for the ingress scenario, with the main difference that in this case the fitting error would be negligible. In addition, an eventual filter central frequency shift can be detected from the TF, for example employing the centre of mass approach, presented in [15], at every node.

On the other hand, as we mentioned in Section 1, signal related parameters are not directly monitorable, since the filters tend to hide several of the signals original characteristics, making traditional monitoring techniques ineffective. Thus, parameters such as the signal 3/6-dB bandwidth and the associated ASE noise (correlated with the signal in OSNR metric) are not directly measurable from the optical spectra.

We propose a supervised ML-based method to estimate in-band the ASE noise from optical spectra collected in the egress monitoring scenarios [20,21]. With respect to our previous works [20,21], we enhanced the proposed method dividing the $\mathrm{OCM}_{n+1,e}$ captured PSD by the one captured with $\mathrm{OCM}_{n,e}$ (i.e. neglecting the effects of the cascade up to node *n*) and improving/tuning the employed ML model coefficients. The proposed solution, as a first step, requires the collection of different sets of optical spectra which are then classified according to some particular signal parameters and labeled with their corresponding ASE noise/OSNR values. Leveraging the labeled spectral data, we then train separate ML regression models for the different classes, to predict the OSNR. Our previous results indicated very good prediction performance, for new optical spectra that were not part of the training. Indeed, in [20,21] we already provided a solid performance evaluation of the proposed ML-based solution, using extensive simulation and experimental datasets. Thus, the main goal of this current work is the comparison of the two placement scenarios and their assessment under common simulation and experimental datasets.

To formally present the method, we represent an acquired optical spectrum instance with a vector $\boldsymbol{s}$ of length l, and we name its corresponding OSNR value as y. The goal is to find the mapping f, between the spectrum $\boldsymbol{s}$ and its OSNR value y, that is $y = f(\boldsymbol{s})$. To do so, we implement a ML model Q_c, where c represents the group of parameters for which the model is valid (e.g. the roll-off factor, the baud rate of the connection and the nominal filter bandwidth). We then train the ML model with a set of monitored and labeled spectra $(\boldsymbol{S}_c, \boldsymbol{y}_c)$. $\boldsymbol{S}_c$ is a matrix of dimension $l \times m$, which represents the set of optical spectra with the same parameters c, while $\boldsymbol{y}_c$ is the vector of length m, of their corresponding OSNR values. Note that, the aforementioned parameters c corresponds to nominal transponders and filter values, so we could create the training set in a calibration phase in the lab or in the field, before commissioning a connection. We also denote by $\hat{\boldsymbol{y}}_c = Q_c(\boldsymbol{S}_c)$ the vector representing the estimated OSNR values and by $\boldsymbol{\varepsilon}_c = \hat{\boldsymbol{y}}_c - \boldsymbol{y}_c$ the estimation errors. The goal of the training process is to identify the model Q_c, which minimizes some function related to the estimation errors $\boldsymbol{\varepsilon}_c$, such as the mean squared error (MSE) function. Once the ML algorithm is trained with the spectra $\boldsymbol{S}_c$ and their reference OSNR values $\boldsymbol{y}_c$, it will be able to return the estimated OSNR value $\hat{y}_c^h$ of an operating channel h with the same parameters c, from its optical spectrum $\boldsymbol{s}$.

3. SIMULATIONS AND RESULTS

A. Simulation setup

To simulate both the ingress and the egress monitoring placement scenarios and to also evaluate the effect of monitors resolution, we implemented the VPIphotonics [27] setup depicted in Fig. 5. We

Table 1. The spans number and the filter parameters for the 16 considered cases

Links (# of spans)				Filters (6-dB bandwidth [GHz] + central freq. shift [GHz])		
0-1	1-2	2-3	3-4	1	2	3
5	2	2	3	37.5+0	37.5+2	37.5+1
				37.5+1	37.5+2	37.5+2
				37.5+2	37.5+1	37.5+0
				37.5+2	37.5-1	37.5+2
2	5	2	3	37.5+0	37.5+2	37.5+1
				37.5+1	37.5+2	37.5+2
				37.5+2	37.5+1	37.5+0
				37.5+2	37.5-1	37.5+2
2	5	2	3	36.5+0	36.5+2	36.5+1
				36.5+1	36.5+2	36.5+2
				36.5+2	36.5+1	36.5+0
				36.5+2	36.5-1	36.5+2
2	5	2	3	38.5+0	38.5+2	38.5+1
				38.5+1	38.5+2	38.5+2
				38.5+2	38.5+1	38.5+0
				38.5+2	38.5-1	38.5+2

Table 2. Estimation accuracy of the filter related features in the simulation case for the ingress placement scenario

Node	Estimated Feature	MSE	σ [GHz]	MIN [GHz]	MAX [GHZ]
1	Centr. freq. shift	0.0019	0.0334	-0.0391	0.0655
	6-dB BW	0.0183	0.0807	-0.0249	0.1937
2	Centr. freq. shift	0.0008	0.0178	-0.0147	0.0454
	6-dB BW	0.0024	0.0479	-0.1057	0.0672
3	Centr. freq. shift	0.0026	0.0482	-0.0702	0.0997
	6-dB BW	0.0163	0.1247	-0.1470	0.2962

generated a 32 GBd polarization multiplexed-quadrature phase shift keying (PM-QPSK) modulated signal, with 0.1 roll-off factor, centered at 193.4 THz (1550.116 nm). In order to simulate the optical links, after the transmitter (TX) we cascaded a number of spans which included 80 km length standard single mode fibers (SSMFs) and erbium-doped fiber amplifiers (EDFAs) with 5 dB noise figure (NF). We set the output power of the TX to 0 dBm as well as the output power of all the EDFAs. Taking into account that the optimum launch power varies depending on several factors (i.e. the amount of ASE noise, the attenuation of the fiber, the amplifier's NF and the NLIs), we chose 0 dBm bearing in mind the specific single channel configuration we considered. Varying the number of fiber spans and EDFAs, we were able to simulate different ASE noise levels and therefore different OSNR values. Each link was followed by an optical node, which we implemented as a cascade of 2 optical filters, with 2nd order Gaussian TFs. We assumed that the 2 optical filters of every node had the same characteristics, in fact our method considers the two filters as an equivalent one, as discussed in Section 2.A. For each equivalent filter, we considered different 6-dB bandwidth values. In addition, in order to emulate the impairment due to the laser drift or filter shift, we also shifted the central frequency of each filter with respect to the TX laser's frequency. Finally, with the aim of covering both the ingress and the egress scenarios, we placed an OCM at the input and at the output of every node of the setup. The spectral resolution of all the employed OCMs was 1 GHz, while the spectral sampling resolution of the collected spectra was 15.625 MHz. This value represented the reciprocal of the time window set in VPI, which was directly correlated to the bitrate value (i.e. 128 Gb/s).

In total, our simulation setup included 3 nodes, 4 links and 7 OCMs: 4 OCMs were used to collect the optical spectra for the ingress scenario model (the blue blocks in Fig. 5), while the remaining 3 for the egress model (the red blocks in Fig. 5). Table 1 summarizes the 16 cases considered: we list there the number of fiber spans and EDFA per link, and the 6-dB bandwidth and central frequency shift of each filter. The number of fiber spans and EDFAs for each link varied and were chosen with the following values: 2, 3 and 5. Varying this value, allowed us to have different ASE noise levels at the input ports of the filters. Additionally, to replicate the narrowing of the filter bandwidth introduced by the filter cascading effect (FCE) and also to take into account imperfections in the production and variation in the ageing conditions, we assigned the following values to the filters 6-dB bandwidths: 36.5 GHz, 37.5 GHz and 38.5 GHz. Finally, to replicate the misalignment between the laser and the filter central frequencies, due to imperfections and ageing, we assumed for each filter a shift which ranged between -2 GHz and +2 GHz.

B. Ingress scenario results

We considered the setup depicted in Fig. 5 for the ingress scenario. There, the only available monitors were the blue ones, i.e. $OCM_{n,i}$, where $n \in [1,4]$ represents the node before which the monitor was placed. Following the method presented in Section 2.A for the filter parameters detection in the ingress scenario, we first retrieved the noisy TFs of the filters corresponding to each node of the setup, which are Node 1, Node 2 and Node 3 for the 16 cases listed in Table 1. Then, after the noise identification and removal process, we fit the resulting portions of spectra with the logarithmic squared version of Eq. 2. Observing the values assumed by the parameters of Eq. 2, in particular the parameters β and δ, we were able to estimate the filter 6-dB bandwidth and the filter central frequency shift, respectively. Finally, we compared the values returned by the algorithm with those reported in Table 1 and calculated the estimation errors. In Table 2 we list the standard deviation (σ), the MSE, the minimum (MIN) and the maximum (MAX) errors for the estimation of the 6-dB filter bandwidth and the filter central frequency shift for the three nodes. Dividing (in the linear domain) the PSD acquired at $OCM_{3,i}$ by the one acquired at $OCM_{2,i}$, should nullify the effect of the path up to $OCM_{2,i}$ location. Nevertheless, the estimation errors reported in Table 2 indicate a small effect of the cascade. In fact, the estimation error for Node *3* was slightly higher than those corresponding to the other two nodes. In general, at Node *1* and Node *2*, the spectra are almost not affected by the cascade effect and the estimation errors are also very low. Therefore, keeping the same accuracy of the first two nodes, as the cascade of links increases, is very hard.

C. Egress scenario results

To study the egress scenario, we considered a particular case of the simulation setup shown in Fig. 5. The monitors available are only the red ones, i.e. $OCM_{n,e}$, where $n \in [1,4]$ represents the node whose egress port is monitored by the OCM. On the spectra captured with these monitors, we applied the ML-based method described in Section 2.B for the in-band ASE noise estimation in the egress scenario. To do so, we leveraged the SVM regression algorithm, a kernel-based nonparametric ML technique. In this study, we formulated the estimation as a regression problem. Training the SVM model using a linear kernel function returned better performance than training it with a Gaussian one, therefore for the training process, we considered the former one. In

Table 3. Estimation accuracy of the ASE noise in the egress placement scenario

	MSE	MIN [dB]	MAX [dB]
Simulation	0.0018	-0.3134	0.6013
Experiment	0.0136	-0.3911	0.3866

Table 4. The 7 considered experimental cases

	Filter 1 6-dB BW (shift) [GHz]	Link(1,2) VOA_1 [dB]	Filter 2 6-dB BW (shift) [GHz]	Link(2,3) VOA_2 [dB]
1	74 (-2)	0	73, 75, 77 (-1, 0, +1)	10
2	74 (-2)	0	73, 75, 77 (-1, 0, +1)	20
3	74 (-2)	10	73, 75, 77 (-1, 0, +1)	10
4	69 (-2)	10	73, 75, 77 (-1, 0, +1)	10
5	74 (-2)	5	73, 75, 77 (-1, 0, +1)	10
6	74 (-2)	2.5	73, 75, 77 (-1, 0, +1)	15
7	69 (-2)	7.5	73, 75, 77 (-1, 0, +1)	20

order to label the training spectra and to evaluate the accuracy of the estimation, we measured the ASE noise values that were used as reference, directly on the spectra collected through the $OCM_{n,i}$, at the ingress port of every node. For the calculation of the noise spectral density integral, we considered a reference noise bandwidth equal to 12.5 GHz (0.1 nm). The total number of spectra that we used was 48 (16 for each one of the nodes): we used the 80% of these spectral data to train the model, the 10% to cross-validate it and the remaining 10% to test it. The cross-validation was used to tune the parameter ε of the SVM regression model. ε represents half the width of the insensitive band, i.e. that tolerance area where no-penalty is assigned to the errors. In addition, to precisely assess the estimation accuracy of the model, we also randomly shuffled the training and the testing data sets 4000 times, trained a different model each time and tested it with its corresponding testing set. The MSE, the MIN and the MAX estimation errors are summarized in Table 3. We achieved a maximum absolute error (MAE) lower than 0.61 dB and a MSE of 0.0018 for the estimation of the ASE noise in the egress scenario. These results reflect the goodness of our approach, also considering that the spectral set we used referred to a setup where we tuned the filter 6-dB bandwidth, while in the past we always considered the 3-dB bandwidth of the filters.

4. EXPERIMENTAL SETUP AND RESULTS

A. Experimental setup

For a further validation of the proposed approaches, we also implemented the experimental setup shown in Fig. 6. By means of a tunable laser working at 193.4 THz (1550.116 nm), we generated a 64 GBd PM-QPSK modulated signal with two different roll-off factors: 0.1 and 0.2. We set the TX output power to -11 dBm. With the aim of

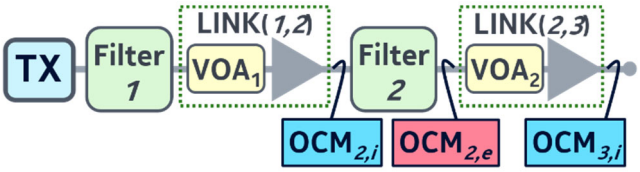

Fig. 6. Scheme of the experimental setup. TX: transmitter; VOA: variable optical attenuator; OCM: optical channel monitor.

emulating the FCE that can occur in a network, right after the TX we placed a first optical filter, namely Filter *1*, through which we simulated this kind of behavior narrowing its 6-dB bandwidth. After this first filter, in order to emulate optical links of different lengths and therefore different ASE noise contributions, we cascaded a variable optical attenuator (VOA) and an EDFA operating in power control mode with output power set to 0 dBm and NF of 5 dB. These 2 blocks together represented link (*1,2*) in Fig. 6. As per the simulation setup, we chose such output power considering the single channel configuration we planned. Following the first link, we placed a second optical filter, namely Filter *2*, the filter on which we tested the proposed models. Thus, we varied its 6-dB bandwidth and its central frequency to generate a number of different possible impairment cases. After Filter *2*, we cascaded a second link, composed by a VOA and an EDFA, to simulate the link after which we place the OCM in the ingress scenario. Finally, three OCMs were placed in the setup: the two related with the ingress scenario (namely $OCM_{2,i}$ and $OCM_{3,i}$), at the end of the two links, and the one for the egress scenario, at Filter *2* output, namely $OCM_{2,e}$. The monitor we used, was the Finisar WaveAnalyzer 1500S, a high-resolution coherent OSA able to reach resolution up to 150 MHz [28]. In order to simulate the performance of an OCM, we collected all the optical spectra at 2 different resolutions: 600 MHz and 1 GHz. The spectral sampling resolution of the collected spectra was equal to the intrinsic value of the employed Finisar OSA, i.e. 20 MHz [28]. Table 4 shows how we clustered the collected spectra into 7 different cases. Each case consists of 9 sub-cases with different 6-dB filters bandwidths and different link attenuation values. While Filter *1* bandwidth and the attenuations of the two links vary for each case, Filter *2* bandwidth assumes the same values in every cluster. Case 1 represents the "default" situation, with Filter *1* 6-dB bandwidth set at 74 GHz, no (additional) attenuation set in link (*1,2*) and 10 dB attenuation set in link (*2,3*). All the other cases constitute a worsening of case 1: at least one of the 3 varying parameters (Filter *1* bandwidth, VOA_1 and VOA_2) assumes a value worse than in the default case. In total, for each of the two roll-off values and resolutions, we collected 189 optical spectra, 63 for each OCM in the setup.

B. Ingress scenario results

As per the simulation scenario, also for the experimental ingress scenario, we retrieved the filter TF following the steps described in Section 2.A. We considered the setup depicted in Fig. 6 with the monitors associated to the ingress scenario, that are $OCM_{2,i}$ and $OCM_{3,i}$. We also used $OCM_{2,e}$ to retrieve the TF to be used as reference for the evaluation of the estimation accuracy. The estimation errors for the 6-dB filter bandwidth and the filter central frequency shift are shown in Fig. 7 and Fig. 8 for roll-off factor of 0.1 and in Fig. 9 and Fig. 10 for roll-off factor of 0.2. The box and whiskers plots graphically represent the mean errors, the standard deviations and the MIN and MAX estimation errors, for each one of the 7 considered cases. From the presented results, it is clear how the default case (i.e. case 1), showed the best performance, especially for the filter bandwidth estimation. On the other hand, when considering the cases with narrower Filter *1*

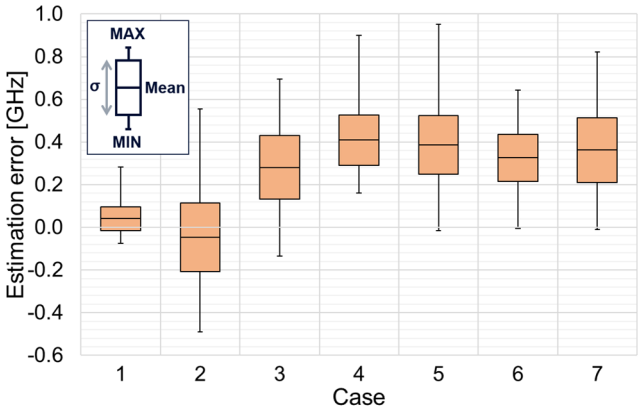

Fig. 7. 6-dB filter bandwidth estimation errors for the 7 experimental cases, with rolloff factor = 0.1.

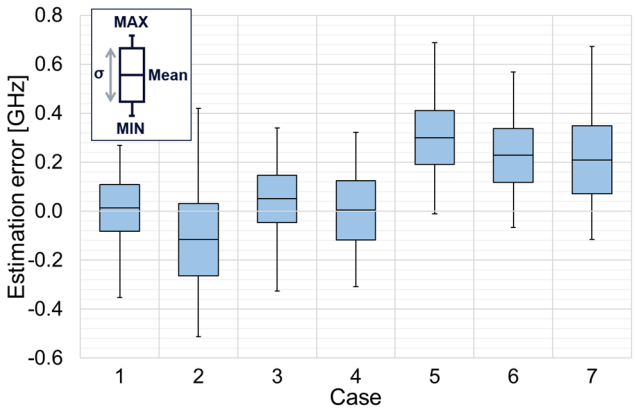

Fig. 9. 6-dB filter bandwidth estimation errors for the 7 experimental cases, with rolloff factor = 0.2.

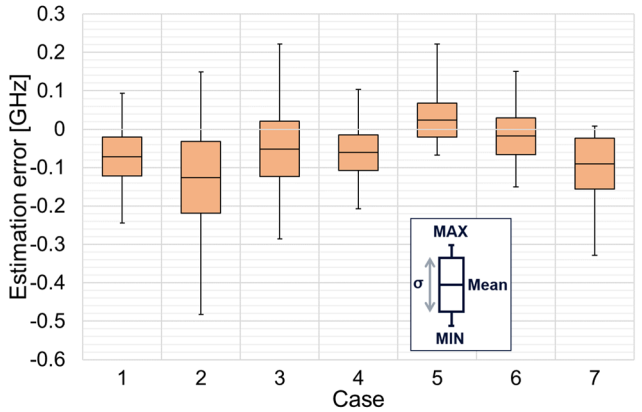

Fig. 8. Filter central frequency shift estimation errors for the 7 experimental cases, with rolloff factor = 0.1.

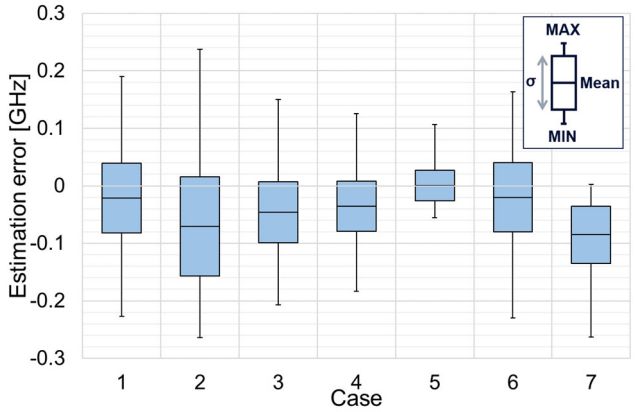

Fig. 10. Filter central frequency shift estimation errors for the 7 experimental cases, with rolloff factor = 0.2.

bandwidth (i.e. cases 4 and 7) or higher links attenuation values (i.e. cases 2 and 7), the estimation accuracy tends to degrade. In general, the accuracy of the 6-dB filter bandwidth estimation was lower compared to the accuracy of the filter central frequency shift, for both the roll-off values. All the results we presented here were obtained with spectra collected at 600 MHz resolution. We did not observe any substantial difference in the estimation accuracy using spectra at 1 GHz resolution.

C. Egress scenario results

As we did for the simulation case, we exploit the optical spectra collected through the experimental setup shown in Fig. 6, to test the egress scenario method for the ASE noise estimation presented in Section 2.B. The optical spectra we considered for the tests were those related to 0.1 roll-off factor, 74 GHz Filter *1* 6-dB bandwidth and OCM spectral resolution of 600 MHz, resulting in a total of 45 optical spectra. As per the simulation case, we retrieved the noise values to be used as reference, calculating the noise spectral density integrals on the optical spectra collected through the ingress placed monitors. In particular, we considered a reference noise bandwidth equal to 12.5 GHz (0.1 nm). Again, we employed SVM regression algorithm, using the 80% of the total spectral data for training the model, the 10% to cross-validate it and the remaining 10% for testing it, randomly shuffling the spectra 4000 times. Also for the experimental case, we used the cross-validation to tune ε, the parameter representing half the width of the insensitive band. The results of the estimation are reported in Table 3. We achieved a MAE lower than 0.4 dB and a MSE of 0.0136. Again, as per the simulated case, it is important to stress that the filter bandwidth we considered in the experimental setup were referring to the 6-dB measured values. Therefore, with respect to the works we carried out in the past [20,21], the effects of the filters on the noise were way more visible this time, since their 3-dB bandwidths were narrower. Nevertheless, comparing our current results with a similar case we had in [21] (i.e. PM-QPSK signal with 0.1 roll-off, 64 GBd baud rate and 72 GHz 3-dB bandwidth), we improved the accuracy of the ASE noise estimation. In fact, in the considered case of [21], the ASE noise estimation MAE was almost 1 dB. In addition, since in [21] we used optical spectra collected with a spectral resolution of 150 MHz, we again did not observe any dependency of the proposed method on the OSA spectral resolution.

5. OCM PLACEMENT SCENARIOS COMPARISON

In the two studied monitor placement scenarios, the estimated parameters have different units of measurement. Therefore, in order to compare them, we converted each estimation error into a percentage with respect to its nominal value, translating the MAEs into relative errors. To do so, the first step is to identify the values to be used as references. For the ingress scenario, the datasheet of the Finisar filter we used in the lab reported a central frequency setting accuracy of ±2.5 GHz and a bandwidth setting accuracy of ±5 GHz [29]. WSSs deployed in real

Table 5. Error ranges and relative errors comparison of the different scenarios

Setup	Scenario	Parameter	Roll-off factor	Parameter error range	Reference error range	Relative error
Simulation	Ingress	Filter central freq. shift	0.1	0.17 GHz	4 GHz	4.3 %
		Filter 6-dB bandwidth	0.1	0.44 GHz	4 GHz	11 %
	Egress	ASE noise	0.1	0.91 dB	1 dB	91 %
Experimental	Ingress	Filter central freq. shift	0.1	0.63 GHz	4 GHz	15.8 %
			0.2	0.5 GHz	4 GHz	12.5 %
		Filter 6-dB bandwidth	0.1	1 GHz	4 GHz	25 %
			0.2	0.93 GHz	4 GHz	23.3 %
	Egress	ASE noise	0.1	0.78 dB	1 dB	78 %

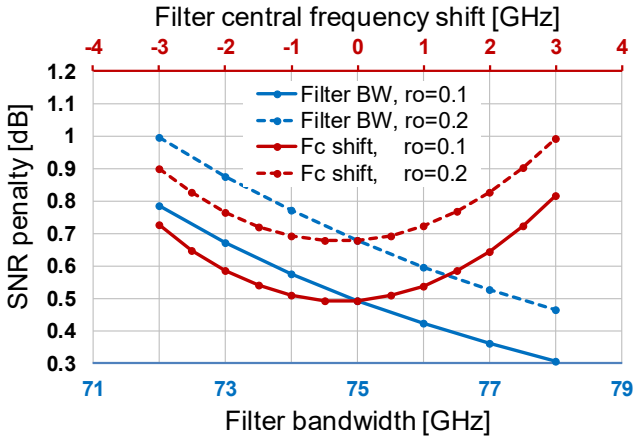

Fig. 11. SNR penalty introduced by a 3.5th order Gaussian filter, as function of its central frequency shift and its bandwidth variation, for an input 64 GBd QPSK signal, with roll-off factor equal to 0.1 and 0.2.

networks could have better characteristics, therefore we decided to adopt for both the filter-related parameters a reference accuracy equal to ±2 GHz [7,15]. For the egress scenario, we obtained a reference for the OSNR/ASE noise estimation, evaluating the amplifier NF, as follows. We considered the cascade of a number of fiber spans with EDFAs at the end of each one of them. We assumed the EDFAs to have a NF equal to 5 dB, with fluctuations of ±0.5 dB [30,31]. This assumption yielded a noise reference error with a 1 dB range.

Then, relying on the filter and signal-related parameters estimation errors reported in Section 3 and in Section 4, we calculated the worst case error ranges and the relative errors with respect to the above references. The results of these calculations are reported in Table 5. Concerning the experimental results, we found that the ingress monitoring strategy improved the filter central frequency estimation by a factor greater than the 84% for roll-off value of 0.1 and by a factor greater than the 87% for 0.2 roll-off. These improvements are with respect to the scenario where no monitoring strategy is implemented and the nominal parameters provided by vendors/datasheets are used. Likewise, the filter 6-dB bandwidth estimation was improved by the 75% for 0.1 roll-off and by a factor greater than the 76% for 0.2 roll-off. On the other hand, the egress monitoring strategy improved the ASE noise estimation accuracy of the 22%, with respect to the case where no optical monitors are employed. Based on the above, we clearly see that the ingress scenario returns higher benefits in terms of reduced uncertainties, with respect to the egress one.

It is worth noting that the relative error is a valuable metric, but not perfectly suitable for eventually evaluating the impact of the network elements on the QoT (e.g. the OSNR/SNR) of the connections. Therefore, to evaluate the QoT estimation related benefits, we translated the parameters estimation errors into SNR estimation errors. In the egress scenario, since we evaluated the improvements in OSNR/noise estimation, there was no need for such a translation. Our proposed egress monitoring and processing method resulted in 0.22 dB improvement in OSNR estimation per link. To obtain a similar metric for the ingress scenario, we simulated in VPIphotonics [27] the transmission of a 64 GBd QPSK modulated signal, with roll-off factor equal to 0.1 and 0.2, crossing a single filter. We measured the SNR penalty introduced by the filter, which we implemented as a 3.5th order Gaussian TF with 75 GHz bandwidth, as function of its central frequency shift and of its bandwidth variation. The results of these simulations are plotted in Fig. 11. Then, using the obtained curves, we calculated the improvement on the SNR penalty estimation. The reference filter-related parameters error ranges (±2 GHz) translated into SNR penalty estimation equal to 0.12 dB for the filter central frequency shift and to 0.16 dB for the filter 6-dB bandwidth. Since the penalty variations for the two different roll-off factors were negligible, we considered them as a unique case. Applying the ingress monitoring strategy and our proposed processing method, we were able to reduce the estimated filter-introduced SNR penalties down to 0.01 dB and 0.03 dB, for the central frequency shift and for the 6-dB bandwidth parameters, respectively. Therefore, our solution yielded a total reduction of the estimated SNR penalty equal to 0.24 dB, for the two considered parameters.

6. CONCLUSION

We studied different scenarios for monitors placement within DWDM and flex-grid optical networks. In particular, we defined an ingress and an egress scenario, in which the monitors are placed before and after the nodes of the network, respectively. In fact, our goal is to minimize the number of employed OCMs optimizing their placement and to enhance the monitoring features with appropriate spectral processing techniques. To this end, we presented two spectral processing techniques which leveraged a curve fitting principle and a ML regression algorithm to retrieve the missing parameters for each scenario: the filter bandwidth and the filter central frequency shift in the ingress, and the ASE noise of the signal in the egress scenario.

We validated the proposed solutions on spectral data generated through simulations and experiments. The obtained results confirmed the validity of the proposed techniques. In particular, in the ingress scenario we observed a MAE lower than 0.98 GHz for the 6-dB bandwidth estimation, and lower than 0.5 GHz for the filter central

frequency shift, with the experimentally generated spectra. Moreover, in the egress scenario, the MAE for the ASE noise estimation was lower than 0.4 dB with the experimental generated spectra.

Comparing the two monitoring scenarios, we identified the ingress one as the most promising solution. In particular, comparing against scenarios where no monitoring strategies are implemented, ingress monitoring improved the filter central frequency and the filter 6-dB bandwidth estimations by 84% and 75% respectively, for a roll-off factor of 0.1. Slightly lower relative estimation errors were observed for a 0.2 roll-off factor. Moreover, translating these estimation improvements into SNR penalties, we obtained a SNR penalty estimation reduction of 92% and 81%, for the filter central frequency shift and for the filter bandwidth, respectively.

In the future, we plan to further evaluate the effects of our proposed monitoring and processing methods in QoT estimation, leveraging also network-wide parameter correlation.

Funding Information. European Union (EU) Horizon 2020 research and innovation programme. Future Optical Network for Innovation Research and Experimentation (ONFIRE) project (765275).

Acknowledgment. The authors would like to thank Fred Buchali, Qian "Theresa" Hu, Karsten Schuh and Ankush Mahajan for lab support.

References

1. E. Riccardi, P. Gunning, Ó. González de Dios, M. Quagliotti, V. Lopez, and A. Lord, "Operator view on the introduction of white boxes into optical networks," J. Lightwave Technol. 36, 3062-3072 (2018).
2. M. Filer, M. Cantono, A. Ferrari, G. Grammel, G. Galimberti, and V. Curri, "Multi-vendor experimental validation of an open source QoT estimator for optical networks," J. Lightwave Technol. 36, 3073-3082 (2018).
3. Z. Dong, F. N. Khan, Q. Sui, K. Zhong, C. Lu, and A. P. T. Lau, "Optical performance monitoring: a review of current and future technologies," J. Lightwave Technol. 34, 525-543 (2016).
4. M. Lonardi, J. Pesic, P. Jennevé, P. Ramantanis, N. Rossi, A. Ghazisaeidi, and S. Bigo, "Optical nonlinearity monitoring and launch power optimization by artificial neural network," J. Lightwave Technol. 38, 2637-2645 (2020).
5. Finisar, "Flexgrid high resolution optical channel monitor (OCM)," 2015, https://optical.communications.ii-vi.com/roadms-wavelength-management/focm01fxc1mn.
6. Viavi, "ROADM and Wavelength Selective Switches," 2019, https://www.viavisolutions.com/en-us/literature/roadm-and-wavelength-selective-switches-application-notes-en.pdf.
7. T. A. Strasser, and J. L. Wagener, "Wavelength-selective switches for ROADM applications," IEEE J. Sel. Top. Quantum Electron. 16, 1150-1157 (2010).
8. R. Shankar, M. Florjańczyk, T. Hall, A. Vukovic, and H. Hua, "Multi-degree ROADM based on wavelength selective switches: architectures and scalability," Opt. Commun. 279, 94–100 (2007).
9. J. M. Fabrega, M. Svaluto Moreolo, L. Martín, A. Chiadò Piat, E. Riccardi, D. Roccato, N. Sambo, F. Cugini, L. Potì, S. Yan, E. Hugues-Salas, D. Simeonidou, M. Gunkel, R. Palmer, S. Fedderwitz, D. Rafique, T. Rahman, H. de Waardt, and A. Napoli, "On the filter narrowing issues in elastic optical networks," J. Opt. Commun. Netw. 8, A23-A33 (2016).
10. IEC 61280-2-9, Optical signal-to-noise ratio measurement for dense wavelength-division multiplexed systems, (2009).
11. B. Collings, "New devices enabling software-defined optical networks," IEEE Commun. Mag. 51(3), 66-71 (2013).
12. M. Filer, and S. Tibuleac, "N-degree ROADM architecture comparison: Broadcast-and-Select versus Route-and-Select in 120 Gb/s DP-QPSK transmission systems," in *Optical Fiber Communication Conference and Exhibition (OFC)* (2014), pp. 1-3.
13. J. Kundrát, O. Havliš, J. Radil, J. Jedlinský, and J. Vojtěch, "Opening up ROADMs: a filterless add/drop module for coherent-detection signals," J. Opt. Commun. Netw. 12, C41-C49 (2020).
14. B. Shariati, M. Ruiz, J. Comellas, and L. Velasco, "Learning from the optical spectrum: failure detection and identification," J. Lightwave Technol. 37, 433-440 (2018).
15. C. Delezoide, P. Layec, and S. Bigo, "Automated alignment between channel and filter cascade," in *Optical Fiber Communication Conference and Exhibition (OFC)* (2019), pp. 1-3.
16. A. Mahajan, K. Christodoulopoulos, R. Martinez, S. Spadaro, and R. Munoz, "Modeling filtering penalties in ROADM-based networks with machine learning for QoT estimation," in *Optical Fiber Communication Conference and Exhibition (OFC)* (2020), pp. 1-3.
17. M. Ruiz, A. Sgambelluri, F. Cugini, and L. Velasco, "Smart filterless optical networks based on optical spectrum analysis," in *21st International Conference on Transparent Optical Networks (ICTON)* (2019), pp. 1–5.
18. D. Wang, M. Zhang, Z. Zhang, J. Li, H. Gao, F. Zhang, and X. Chen, "Machine learning-based multifunctional optical spectrum analysis technique," IEEE Access 7, 19726-19737 (2019).
19. Y. Li, N. Hua, J. Li, Z. Zhong, S. Li, C. Zhao, X. Xue, and X. Zheng, "Optical spectrum feature analysis and recognition for optical network security with machine learning," Opt. Express 27, 24808-24827 (2019).
20. F. Locatelli, K. Christodoulopoulos, J. M. Fabrega, M. Svaluto Moreolo, and S. Spadaro, "Machine learning-based in-band OSNR estimation from optical spectra," Photonics Technology Letters 31, 1929-1932 (2019).
21. F. Locatelli, K. Christodoulopoulos, J. M. Fabrega, M. Svaluto Moreolo, L. Nadal, and S. Spadaro, "Experimental demonstration of a machine learning-based in-band ONSR estimator from optical spectra," in *International Conference on Optical Network Design Modelling (ONDM)* (2020), pp. 1-4.
22. F. Locatelli, K. Christodoulopoulos, J. M. Fabrega, M. Svaluto Moreolo, L. Nadal, and S. Spadaro, "Filter features extraction from optical spectra," in *European Conference on Optical Communication (ECOC)* (2020), pp. 1-4.
23. ITU-T G.694.1, Spectral grids for WDM applications: DWDM frequency grid, (2020).
24. A. Mahajan, K. Christodoulopoulos, R. Martinez, S. Spadaro, and R. Munoz, "Modeling EDFA gain ripple and filter penalties with machine learning for accurate QoT estimation," J. Lightwave Technol. 38, 2616-2629 (2020).
25. K. Christodoulopoulos, C. Delezoide, N. Sambo, A. Kretsis, I. Sartzetakis, A. Sgambelluri, N. Argyris, G. Kanakis, P. Giardina, G. Bernini, D. Roccato, A. Percelsi, R. Morro, H. Avramopoulos, P. Castoldi, P. Layec, and S. Bigo, "Toward efficient, reliable, and autonomous optical networks: the ORCHESTRA solution," J. Opt. Commun. Netw. 11, C10-C24 (2019).
26. C. Pulikkaseril, L. A. Stewart, M. A. F. Roelens, G. W. Baxter, S. Poole, and S. Frisken, "Spectral modeling of channel band shapes in wavelength selective switches," Opt. Express 19, 8458-8470 (2011).
27. VPIphotonics, 2020, https://www.vpiphotonics.com.
28. Finisar, "WaveAnalyzer High-Resolution Optical Spectral Analysis," 2020, https://ii-vi.com/product/waveanalyzer-1500s-high-resolution-optical-spectrum-analyzer.
29. Finisar, "WaveShaper 4000S Multiport Optical Processor," 2014, https://optical.communications.ii-vi.com/sites/default/files/downloads/waveshaper_4000s_product_brief_11_14.pdf.
30. P. Ramantanis, C. Delezoide, P. Layec and S. Bigo, "Revisiting the calculation of performance margins in monitoring-enabled optical networks," J. Opt. Commun. Netw. 11, C67-C75 (2019).
31. Arris, "CHP EDFA Headend Erbium Doped Fiber Amplifiers," 2018, https://www.commscope.com/globalassets/digizuite/61636-chp-edfa.pdf.